

1.1 The K⁺ Beam Line

1.1.1 Rationale

1.1.1.1 Choice of Accelerator and Primary Proton Momentum

Distinct advantages can be gained from performing a charged kaon, ultra-rare decay experiment, $K^{+(-)} \rightarrow \pi^{+(-)} \nu \bar{\nu}$ at high energy and, in particular, at the 400 GeV/c SPS ¹:

From a simple empirical formula, which roughly fits the measured particle production data (1), it can be deduced that, per primary proton of fixed momentum p_0 , the maximum K^+ (K^-) production in a given momentum bite, $\Delta p/p$, and solid angle, $\Delta\Omega$, occurs at momentum: $p_K \sim 0.35 p_0$ ($\sim 0.23 p_0$) and, at a constant fraction of the primary momentum p_K / p_0 : K^+ (K^-) production increases as p_K^2 and therefore as p_0^2 .

It follows that the number of K^+ (K^-) decays in a given fiducial length is maximum for $p_K \sim 0.23 p_0$ ($\sim 0.15 p_0$) and, at constant p_K / p_0 , the number of K^+ (K^-) decays in a given length increases as p_K and therefore as p_0 .

Furthermore, the acceptance, resolution and rejection power of certain detectors, e.g. calorimeters and photon- and muon-veto counters, improve at higher energy.

The principal disadvantage of performing the experiment at high momentum lies in the difficulty of separating the kaons from other charged hadrons in the beam. Thus, in a beam employing radio-frequency cavities to provide transverse dispersion and subsequent cancellation of the deflection for π^+ and protons to be absorbed, the distance between cavities has to increase as p_K^2 . However, the decay length, determining the survival of the wanted kaons increases only as p_K .²

However, even in a relatively short, 'unseparated' beam, it is possible to suppress the positron (electron) component, originating from the production and decay of π^0 in the target and subsequent conversion of the photons. The e^+ (e^-) component has been measured to be ~ 0.2 (~ 0.3) of the total particle flux for $p_K = + (-)60$ GeV/c and $p_0 = 400$ GeV/c (1) and varies roughly as $\sim (p_K/p_0)^2$ relative to the π^+ (π^-) in the beam.

1.1.1.2 Choice of K⁺

A choice of a positive rather than a negative kaon beam is motivated by the fact that, at a possible beam momentum of, for example, 75 GeV/c (Section 1.1.1.3), the ratio of production rates:

1 400 GeV/c is the highest proton momentum, at which the SPS can sustain a duty cycle of ≈ 0.3 .

2 In the case of the 22 GeV/c K^+ beam proposed at FNAL (12), super-conducting r.f. cavities operating at a frequency of 4 GHz would be employed to suppress the π^+ and protons by at least an order of magnitude. The beam would have a total length of 216m, leading to a K^+ survival factor of only ≈ 0.27 , compounded by losses inherent in the separation mechanism.

K^+ / K^- per 400 GeV/c proton is ≈ 2.1 and the ratio: $(K^+/\pi^+) / (K^-/\pi^-) = \approx 1.2$, whilst the ratio: $(K^+ / \text{Total positively-charged particles}) / (K^- / \text{Total negatively-charged particles}) = \approx 1.0$.

1.1.1.3 Choice of Beam Momentum

The choice of $p_K = +75 \text{ GeV/c}$ as the central beam momentum is suggested with regard to the criteria listed in Table 1. The entries are shown for momenta of 60 and 120 GeV/c, at which complete measurements of particle production by 400 GeV/c protons on Be targets are available (1), and at 75 GeV/c, for which the relative particle composition was determined in 2007 and the absolute yield by interpolation of the data in (1).

Moreover, the ‘useful’ range of momenta for a π^+ from K^+ decay to be distinguished from background μ^+ and hence to be accepted by the RICH detector is: $\sim 15 < p_\pi < 35 \text{ GeV/c}$. In the decay of a K^+ at 75 GeV/c, particles, other than neutrinos, associated with an accepted π^+ must therefore carry an energy $\geq 40 \text{ GeV}$, sufficient to prevent their escape without detection.

Finally, 75 GeV/c proves to be near to the maximum momentum, for which the essential functions which are required of the beam (described in Sections 1.1.2.3 - 1.1.2.7) can be accomplished, with close packing of the elements, in the available length of $\sim 102\text{m}$ from production target to the beginning of the decay fiducial region.

1.1.2 The High-Intensity K^+ Beam

1.1.2.1 Primary Proton Beam

The primary proton beam used for the production of the high-intensity K^+ beam has previously served to produce the K_L^0 and the K^+ and K^- beams for experiments NA48 (2) and NA48/2 (3), respectively.

The 400 GeV/c, slow-extracted, proton beam from the SPS to the North Area is split into three branches to impinge on each of three targets (T2, T4, T6), to produce beams of secondary particles in an underground target cavern (TCC2). Target station T4 is the source of two secondary beams, H8 and H6. Magnets before and after the target allow the protons that have not interacted to be directed towards the front end of a third beam line, P42, for a wide range of choices of momenta in the two secondary beams³. The P42 beam is designed to transport the protons (through tunnels TT83, TDC8 and TT85) over a distance of $\sim 823\text{m}$ to the entrance of the North Area High Intensity Facility (NAHIF) (4)⁴. This comprises the enlarged underground target/beam tunnel, TCC8, and the

³ When required, different settings of the T4 target station magnets allow neutral particles to be directed towards the P42 beam line. Electrons (or positrons), from conversion of photons in a thin lead sheet, can then be selected with narrow momentum band ($\approx \pm 0.1\% \Delta p_e/p_e$) around chosen central momenta (typically, $10 < p_e < 100 \text{ GeV/c}$) and transported to the detectors via the P42 and K12 lines.

⁴ An alternative path for the protons is available via target T6 (along a beam line, P62, which, after the first $\approx 130\text{m}$, joins and thereafter follows the same path as P42), on condition that the front-end (pion decay section) of the M2 muon beam from target T6 is set to a momentum of -200 GeV/c for $+400 \text{ GeV/c}$ in P62.

experiment cavern, ECN3. A drawing of the beam layout in the SPS North Area is available (5) and Figure 1 schematically shows the optics of the P42 beam.

Table 1 Criteria for the choice of the beam momentum.

Beam Characteristics		60 [GV/c]	75 [GeV/c]	120 [GeV/c]
Fluxes at production in 42 μ ster $\Delta\Omega$. % $\Delta p/p$ acceptance / 10^{12} incident protons per s	p $\times 10^6$	89	171	550
	K^+ $\times 10^6$	40	53	71
	π^+ $\times 10^6$	353	532	825
	Total $\times 10^6$	482	756	1446
Survival factor over 102m	K^+	0.797	0.834	0.893
	π^+	0.970	0.976	0.985
Fluxes at 102m from target in 42 μ ster $\Delta\Omega$. % $\Delta p/p$ acceptance / 10^{12} incident protons per s	p $\times 10^6$	89	173	550
	K^+ $\times 10^6$	32	45	63
	π^+ $\times 10^6$	343	525	813
	Total $\times 10^6$	464	743	1426
Decays in 60m fiducial length / 10^{12} incident protons per s ⁵	K^+ $\times 10^6$	3.9	4.5	4.1
	π^+ $\times 10^6$	6.1	7.4	7.2
K^+ decays / π^+ decays in 60m ⁶		0.64	0.61	0.57
K^+ decays in 60m / Total hadron flux ⁷	$\times 10^{-3}$	8.4	6.1	2.9
$K^+ \rightarrow \pi^+ \nu \bar{\nu}$ Acceptance (Region I, no p_π cut)		0.08	0.11	0.11
Accepted $K^+ \rightarrow \pi^+ \nu \bar{\nu}$ / 10^{12} protons per s	$\times 10^6 \times \text{B.R.}$	0.31	0.50	0.45
Accepted $K^+ \rightarrow \pi^+ \nu \bar{\nu}$ / π^+ decays in 60m ⁶	$\times \text{B.R.}$	0.052	0.067	0.062
Accepted $K^+ \rightarrow \pi^+ \nu \bar{\nu}$ / Total hadron flux ⁷	$\times 10^{-3} \times \text{B.R.}$	0.67	0.67	0.31

⁵ The K^+ decay rate relative to incident protons is related to the Signal with respect to the accompanying Background (notably neutrons and muons) resulting from primary protons interacting in the target and beam dump.

⁶ The ratio of K^+ to π^+ decay rates is related to the Signal to Background of decay products in the detectors.

⁷ The K^+ decay rate relative to the total hadron beam rate is related to the Signal available for a given (limiting) particle flux through the beam-defining detectors used for particle identification (CEDAR) and tracking and momentum measurement (GigaTracker).

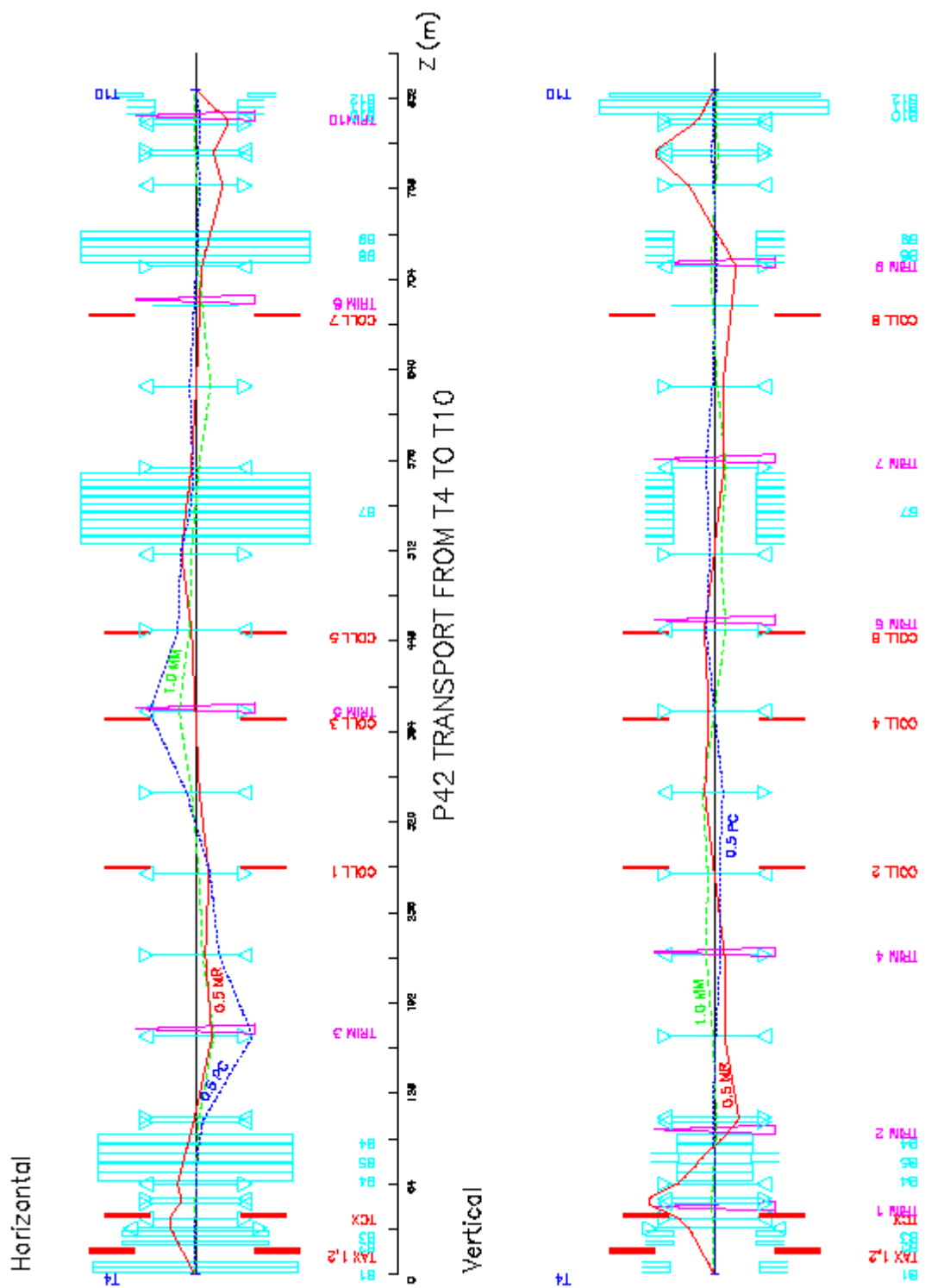


Figure 1 Schematic Optics of the primary proton beam [P42]

At the exit of target station T4, the transmitted proton beam passes through apertures in two vertically-motorized beam-dump/collimator modules, TAX 1 and TAX 2 of beam P42 (XTAX043018, XTAX043020), in which holes of different apertures define the angular acceptance of the beam and hence allow the flux of protons to be selected over a wide range. Moreover, access to the zones TCC8 and ECN3 is governed by closing TAX 1 and 2 in conjunction with switching off two magnets at the front of the beam. Table 2 lists the combinations of apertures available in TAX 1 and 2 for the proton beam and the corresponding transmission factors. The 'Range' refers to a possible restriction, which can be imposed on the movement of each TAX and hence on the apertures that may be selected, so as to guard against unwanted high proton fluxes being transmitted.

To prevent the primary beam from causing damage to components, a computer surveillance program (*PO-SURVEY*) allows the currents in the principal magnets of the P42 beam line to be monitored and, in case of error (or bad reading), automatically causes TAX 2 to close. This surveillance is usually extended to include critical magnets in the kaon beam line, K12, to prevent the secondary beam from passing into the detectors of the experiment.

Table 2 Apertures and Positions of TAX 1 and TAX 2 of Beam P42

Apertures and Vertical Positions of TAX 1			TAX 2 of Beam P42			
Diameter ∅ (mm)	Position y (mm)	Range	Diameter ∅ (mm)	Position y (mm)	Range	Transmission factor
14.0	-81	Medium	12.0	-21	Medium	1.0
14.0	-81	Medium	10.0	+19	Medium	~0.8
7.5	-21	Medium	10.0	+19	Medium	~0.5
7.5	-21	Medium	4.0	+59	Small	~0.12
7.5	-21	Medium	2.0	+99	Small	~0.03
--	+140	Small	--	+140	Small	<i>No Beam (Access)</i>

1.1.2.2 Secondary Beam Layout and Design

The secondary hadron beam, 'K12HIKA+', is designed to be derived from a high, but attainable, flux of 400 GeV/c protons (Section 1.1.2.10) in the underground North Area High Intensity Facility. The target/beam tunnel, TCC8, and the cavern, ECN3, where the detectors of experiment NA48 have been installed, have a combined length of 270m. It is planned to reuse the existing target station, T10, (located 15m from the beginning of TCC8), and to install the secondary beam along the existing (straight) K12 beam line, of length 102m to the exit of the final collimator, which marks the

beginning of the decay fiducial region and points to the NA48 detectors (notably the liquid krypton electro-magnetic calorimeter, LKR). A listing of the order and geometry of all elements along the new beam for experiment NA62 is contained in an updated *BEATCH* output file, accessible from (6) under the heading: K12HIKA+ and a drawing of the layout of the beam and detectors is available (7). Figure 2 schematically shows the beam optics, calculated using the programme *TRANSPORT* (8), corresponding to the updated output file also accessible from (6).

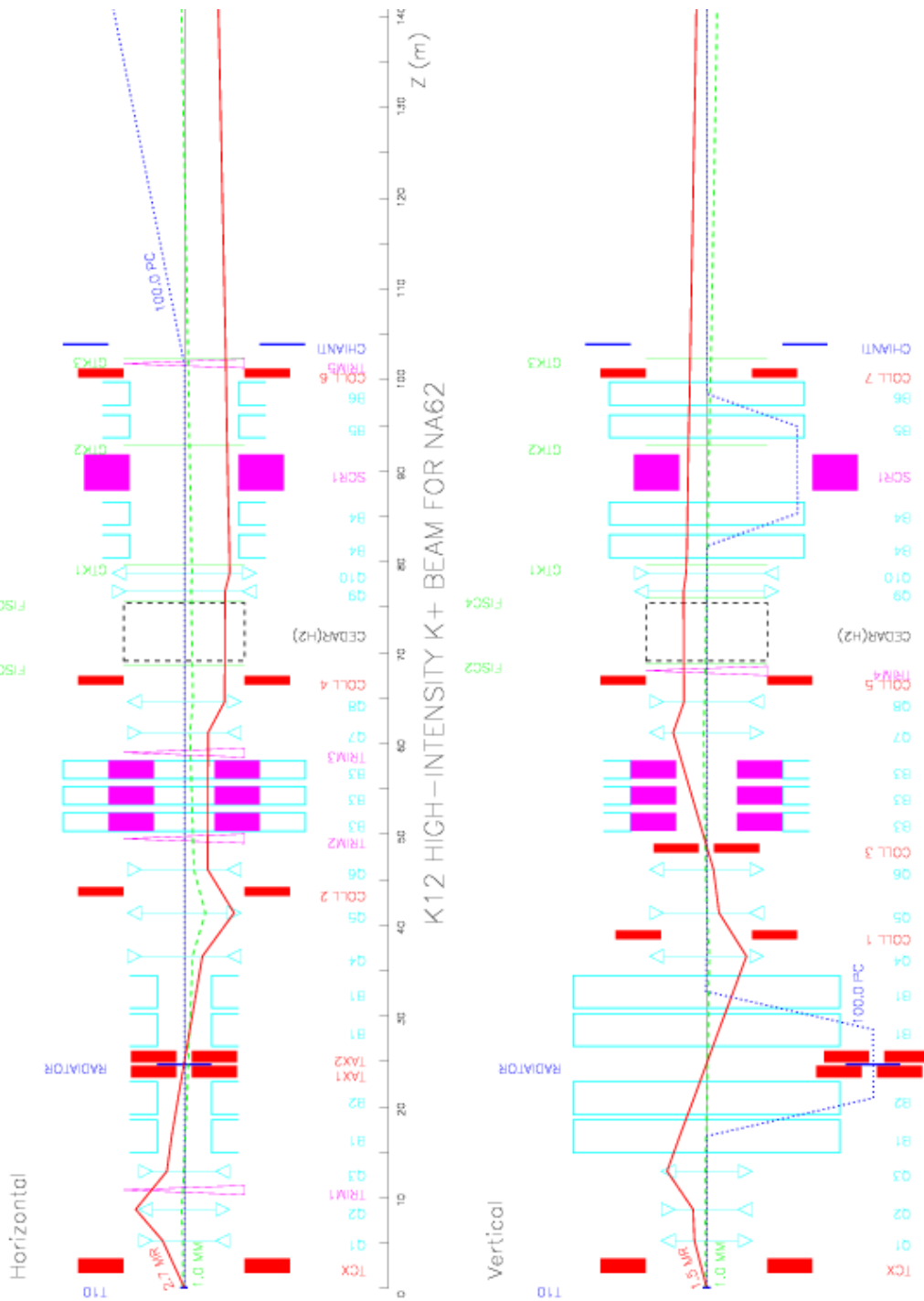


Figure 2 Schematic layout and optics of the high intensity K^+ Beam (K12HIKA+).

1.1.2.3 Targeting

The primary protons, transported via the P42 beam line, are focused and directed at zero angle⁸ onto a 400mm long, 2mm diameter, beryllium target. This is suspended between thin aluminium foils and is cooled by forced convection of air in the T10 target station. The target is followed by a 950mm long, water-cooled, copper collimator, offering a choice of bores of different apertures. The largest, 15mm in diameter, is generally selected to transmit the wanted secondary particles as well as the remaining primary proton beam. Unwanted particles (notably π^\pm , K^\pm) issuing from the target at angles $> \sim 6$ mrad are thereby absorbed before they can decay to muons. Following the vacuum entrance window (0.1 mm thick aluminium), the opening angle for the transmitted beam is further reduced to ~ 4 mrad by a 1.6m long, collimator (TCX 101003) of 28mm diameter bore.

1.1.2.4 Acceptance, Momentum Selection and Positron Suppression

In contrast to the previous, simultaneous K^+ and K^- beams (3), the first active elements of the high-intensity beam are a triplet of radiation-hard, small-aperture, quadrupole magnets, QUAD 1, 2 and 3 (QNRB101005, QNRB101009, QNRB101013), which collect a large solid angle acceptance (± 1.5 mrad horizontally $\times \pm 2.7$ mrad vertically) at 75 GeV/c central momentum. The quadrupoles are fitted with cylindrical, stainless-steel vacuum tubes of 55mm inside diameter; those in QUAD 2 and QUAD 3 serve to define the acceptance angles in the horizontal and vertical planes, respectively. The drift-space between these two quadrupoles serves to lodge a horizontal steering magnet, TRIM 1 (MDXH101011), used to centre the beam at the longitudinal position between two, vertically-motorized, beam-dump/collimator modules, TAX 1 and TAX 2 of beam K12 (XTAX101024, XTAX101026), where it is brought to a focus in both planes.

Front views of the two TAX modules, each 1.615m long, are shown in Figure 3. They are composed of copper-, followed by iron-blocks, mounted on water-cooled, copper tables, to enable them to absorb the remaining primary proton beam. TAX 1 + TAX 2 are located in a ~ 3.4 m-long space between 0.2mm-thick aluminium vacuum exit and entrance windows, in the middle of a 'front-end achromat'. The achromat consists of four, vertically-deflecting, radiation-hard dipole magnets, BEND 1A, 2, -1B and 1C (MTRV101017, MTRV101021, MTRV101029, MTRV101033). The first and second magnets (with opposite polarity) give the 75 GeV/c beam a parallel downward displacement of 110mm, so as to pass through a set of graduated holes, of smallest diameter 10mm, contained in tungsten-alloy cylinders which are inserted in the blocks of TAX 1 and TAX 2. A list of these blocks and their inserts is shown in Table 3.

⁸ The choice of zero production angle provides the maximum yield (though not the highest fraction) of K^+ per incident proton. In this case, an angle around zero is practically imposed by the need to place strong acceptance quadrupoles of small aperture so close to the target, that the remaining primary proton beam must also pass through their apertures before being dumped.

Table 3 List of blocks and cylindrical, W-alloy, collimator Inserts

TAX 1 (XTAX 101024)					TAX 2 (XTAX 101026)				
Block		Height from base (mm)	Inserts		Block		Height from base (mm)	Inserts	
No	Mat		Outer \varnothing (mm)	Inner \varnothing (mm)	No	Mat		Outer \varnothing (mm)	Inner \varnothing (mm)
1	Cu	742	40	-	1	Fe	742	60	10.0→10.8
		522	40	15.0→13.5			522	60	10.0→10.8
		302	40	15.0→13.5			302	60	-
2	Cu	742	40	-	2	Fe	742	60	11.0→12.0
		522	40	13.2→12.2			522	60	11.0→12.0
		302	40	13.2→12.2			302	60	-
3	Fe	742	40	-	3	Fe	742	60	12.2→13.2
		522	40	12.0→11.0			522	60	12.2→13.2
		302	40	12.0→11.0			302	60	-
4	Fe	742	40	-	4	Fe	742	60	13.5→15.0
		522	40	10.8→10.0			522	60	13.5→15.0
		302	40	10.8→10.0			302	60	-

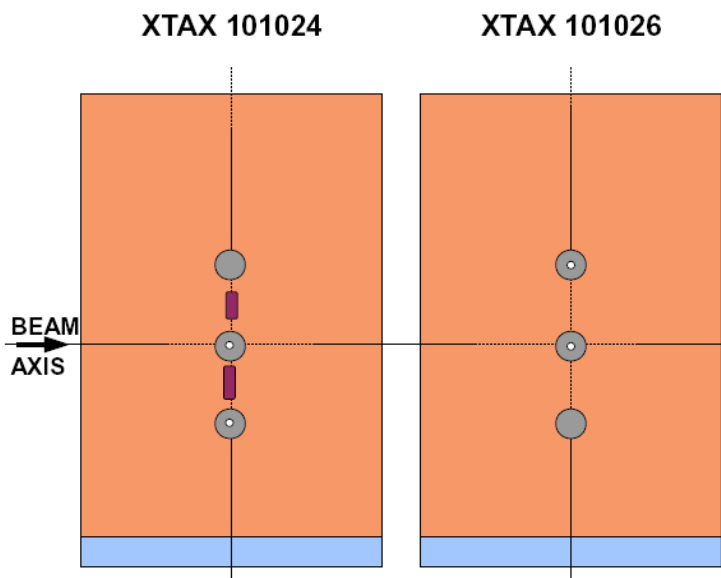


Figure 3 Front view of the beam-dump / collimator modules TAX1 and TAX2 of the K12 Beam.

The combination of vertical positions and permitted ranges of TAX 1 and TAX 2, used to select the 'K+ DOWN' path through the front-end achromat is indicated in Table 4 and is illustrated in Figure 4 (a), together with other combinations, which would allow for different choices of beam mode (discussed in Section 1.1.2.11)⁹. The chosen set of apertures redefines the beam at the focus in the horizontal plane and, by suitable off-set in the vertical plane (also indicated in Table 4), permits a narrow momentum band of $\pm 1.0\% \Delta p/p$ (r.m.s.) to be selected about the central momentum of +75 GeV/c. At this point between the two TAX modules, a motorized mechanism permits a 'radiator' (XCON101025), shown in Figure 5, made of tungsten plates of various thicknesses from 0 up to 5mm ($\sim 1.3 X_0$), to be introduced into the beam. This is designed to cause e+ to lose sufficient energy by Bremsstrahlung to be rejected (with a survival factor down to $\sim 10^{-3}$) after the beam momentum has been redefined (see Table 5). Here the relatively large intrinsic divergences of the beam at the foci ensure that multiple-scattering in the radiator material does not lead to excessive loss of hadrons out of the beam emittance. The third and fourth magnets return the wanted particles onto the undeviated axis and thereby provide the second stage of momentum-definition.

Table 4: Vertical Positions of TAX 1 and TAX 2 for different Modes of Beam K12

TAX 1		TAX 2		
Position y (mm)	Range	Position y (mm) ¹⁰	Range	K12 Beam Mode, Path
-110.0 -107.5	Large	+110.0 +112.5	Small	K12HIKA+ : K⁺ DOWN $\Delta p/p$ (r.m.s.) = 1.0 %
+110.0	Small	-110.0	Large	<i>K UP</i>
+110.0	Small	+110.0	Small	Simultaneous <i>K⁺ DOWN + K UP</i>
0.0	Medium	0.0	Medium	K12HIKOL : <i>K⁰ ON AXIS</i>
+140	Small	+140	Small	MUONS: <i>K-LESS</i> <i>UP+DOWN beams STOPPED</i>

⁹ In this case the TAX 'Ranges' are set to prevent both modules from being moved into a position near 0.0, where the primary proton beam after the target might be transmitted along the subsequent beam line. (For the KOL on axis (Section 2.1.2.11, option 2)), this is prevented by imposing a minimum vertical angle of incidence of the upstream P42 beam – and hence a non-zero production angle for the KOL).

¹⁰ Note for TAX 2, that the y-position is measured with the POSITIVE direction pointing DOWNWARDS !

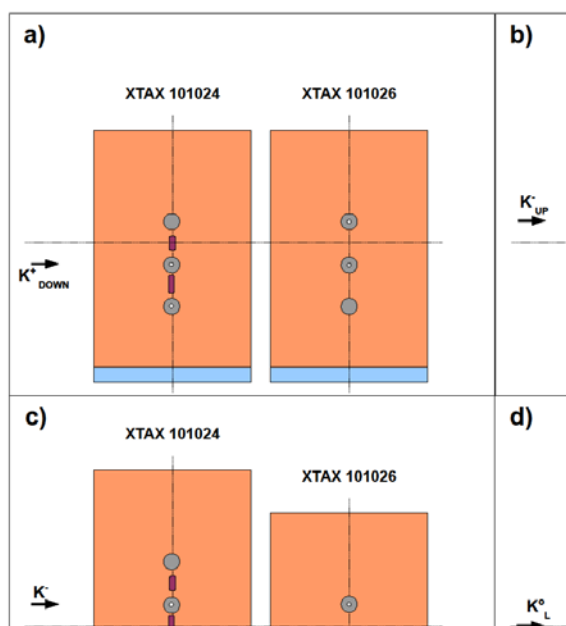


Figure 4 TAX 1 and 2 positions for different selections of K12 Beam modes and paths

- (a) **K12HIKA+** : K^+ DOWN (b) K^+ UP
 (c) Simultaneous K^+ DOWN + K^+ UP (d) **K12HIKOL** : K^0_L ON AXIS

Table 5 Radiator positions and thickness with the corresponding positron (electron) survival factor.

Vertical Position: y (mm)		Thickness of W		e^\pm Survival factor
For K^+ , K^- beam(s):	For K^0_L beam:	(mm)	(X/X_0)	
± 100	0	0	0	1.0
+60	-50	2.0	0.53	~ 0.06
+20	-90	3.0	0.80	~ 0.015
-20	+90	4.0	1.06	~ 0.004
-60	+50	5.0	1.33	~ 0.001

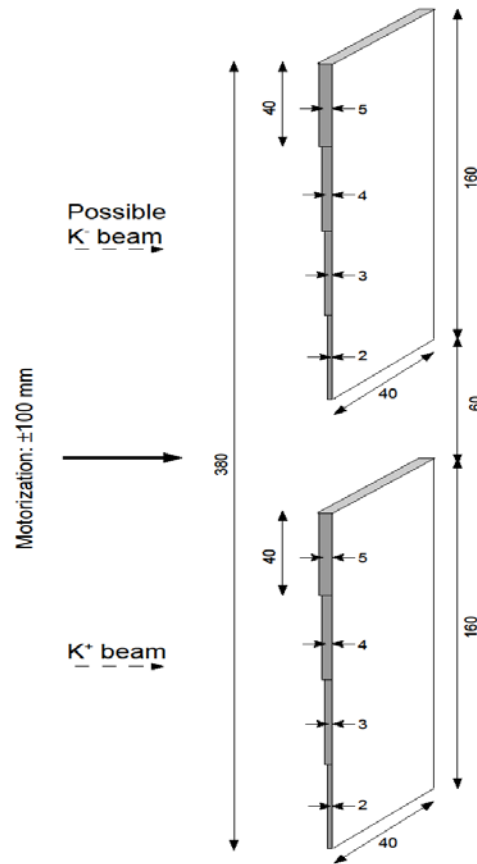


Figure 5 Schematic view of tungsten radiators that can be moved vertically into the beam to absorb positrons (electrons) in the K^+ (K^-) beam.

1.1.2.5 Beam Definition and Muon Sweeping

A triplet of quadrupoles, QUAD 4, 5 and 6 (QNL 101036, QNL 101041, QNL 101046), interspersed by adjustable, vertical and horizontal acceptance-redefining collimators, COLL 1 (XCSV101038) and COLL 2 (XCSH101043), serves to refocus the beam in the vertical plane and to make it parallel and of limited lateral extent in the horizontal plane. This allows it to pass through a 40mm diameter, almost field-free bore, drilled in iron slabs, which are inserted to fill the 200mm high gaps in three, 2m-long, dipole magnets, BEND 3A, 3B and 3C (MBPL101051, MBPL101054, MBPL101057). The vertical magnetic field in the iron surrounding the beam serves to sweep aside muons of both signs, whilst the deviation of the beam due to the small stray-field inside the bore can be cancelled by two steering dipoles, TRIM 2 (MDXH101049) before and TRIM 3 (MDXH101059) after the MBPL magnets. In the vertical plane, an adjustable collimator, COLL 3 (XCSV101048), with tapered jaws open to $\sim \pm 1.2\text{mm}$, shown in Figure 6, is used to redefine the beam at a second focus. At this point the e^+ , that have been degraded in momentum, are displaced sufficiently to be absorbed.

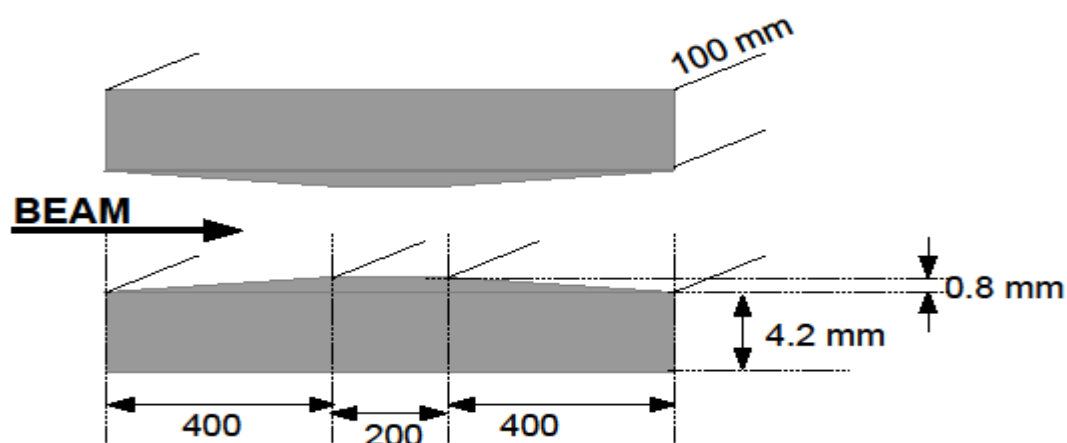


Figure 6 2-jaw collimator (XCSV101048) used to redefine the vertical beam spot

1.1.2.6 K⁺ Tagging

A pair of quadrupoles, QUAD 7 and 8 (QNL 101061, QNL 101065), then renders the beam sufficiently large and parallel in both planes to match the requirements of an upgraded CEDAR differential Čerenkov counter (XCED101072) (9), which can be tuned to tag only the K⁺ in the beam (Chapter 2.2). The CEDAR occupies a length of ~6.0m. To limit the material traversed by the beam to a total of $<7 \times 10^{-3} X_0$, hydrogen gas (at an absolute pressure of ~3.85 bar) is used to fill the CEDAR pressure-vessel. This is connected directly to the beam vacuum tube via flexible bellows at each end. The hydrogen gas volume is separated from the vacuum by thin entry and exit windows of aluminium-alloy, 75mm in diameter. To be sure that a rupture would not affect the detectors of the experiment, the downstream window is designed to be thicker (~0.2mm) than the upstream one (~0.1mm). The upstream window is in contact with the beam-line vacuum only, which is linked to an evacuated vessel of sufficient volume (~4m³) to contain the hydrogen gas at a pressure below atmospheric.

The CEDAR is preceded by an adjustable, 4-jaw (horizontal and vertical) cleaning collimator, COLL 4 / 5 (XCHV101067), and a vertical steering magnet, TRIM 4 (MDXV101068). About 7m apart along the beam and straddling the CEDAR, are two pairs of filament scintillator counters, FISC 1 and 3 (XFFH101069, XFFH101075) and FISC 2 and 4 (XFFV101070, XFFV101076), which, when connected in coincidence respectively, permit the mean divergence of the beam to be measured and tuned to zero in each plane.

1.1.2.7 Beam Tracking and Momentum Measurement

A pair of weakly-focusing quadrupoles, QUAD 9 and 10 (QFS 101077, QFS 101079), matches the beam through the tracking and momentum-measurement stage, shown schematically in Figure 7 and limits the beam size through the apertures of the downstream detectors. The beam tracking system consists of three 'GigaTracker' stations (Chapter 2.3), composed of Si-pixel arrays, each of active area: ±30mm (horizontally) x ±13.5mm (vertically), installed in the beam vacuum, where,

when needed, they can be isolated by separation valves (VXSV101080, VXSV101093 and VXSV $\emptyset=320\text{mm}$). The stations are arranged so that the space between GTK 1 and GTK 3 is occupied by a ‘second achromat’, composed of four, vertically-deflecting, C-shaped dipole magnets, BEND 4A, -4B, 5 and 6 (MCBV101082, MCBV101085, MCBV101095, MCBV101098). Whereas the yokes of the first three magnets are, as usual, below the beam (*Down*), that of the fourth is supported above the beam (*Up*). Use is thereby made of the return fields in the yokes of the third and fourth magnets to supplement the ‘defocusing’ action for μ^+ , produced by a 5m-long, toroidally-magnetized iron collimator, SCRAPER 1 (XCMV101090), which surrounds the beam in the momentum-dispersed section between the second and third magnets. Here, its lower jaw, placed 20mm below the beam, can intercept and deflect away μ^+ of momenta $< \sim 55 \text{ GeV}/c$, which are dispersed out of the 75 GeV/c parent π^+ , K^+ beam. Moreover, the upper jaw blocks the undeviated and upper paths through the achromat, thereby ensuring that no punch-through, neutral (neutrons, K^0_L) or negatively-charged (π^- , K^-), hadrons can be transmitted to the end of the beam. GTK 2 is located in the same section, just after the magnetic collimator, where the +75 GeV/c beam has a parallel, downward displacement of 60mm and a dispersion of $0.6\text{mm} / \% \Delta p/p$ that allows the track momentum to be measured with a resolution of $\approx 0.2 \%$ (also indicated in Figure 7). GTK 3 is placed on the undeviated axis, after a final, adjustable, 4-jaw cleaning collimator, COLL 6 / 7 (XCHV101101), and is followed by a series of ‘guard-ring’ scintillation counters (CHANTI), which surround the beam in vacuum and are designed to veto interactions in the exit layer of GTK 3.

Between the cleaning-collimator and GTK 3, a horizontal steering magnet, TRIM 5 (MDXH101102), is used to deflect the beam away from the straight axis by an angle of +1.2 mrad (towards the Jura). This angle is adjusted, so that the subsequent -3.6mrad deflection, due to the single spectrometer magnet (MNP-33), directs the beam back through the central aperture of the LKR calorimeter, as shown schematically in Figure 8.¹¹

¹¹ The +1.2 mr horizontal deflection causes a small dispersion in angle as a function of momentum of the beam entering the fiducial region: $\Delta x' \text{ (mr)} = -0.012 \Delta p/p \text{ (\%)}$. For $dp/p \text{ (r.m.s.)} = 1.0 \%$, the contribution to the angular spread of the beam, $\Delta x' \text{ (r.m.s.)} = 0.012 \text{ mr}$, is small compared to its intrinsic divergence (Table 6). Using the measured momenta (Figure 12), the contribution to the error on the angle measurements of individual tracks, $dx' \text{ (r.m.s.)} = \approx 0.003 \text{ mr}$, becomes negligible.

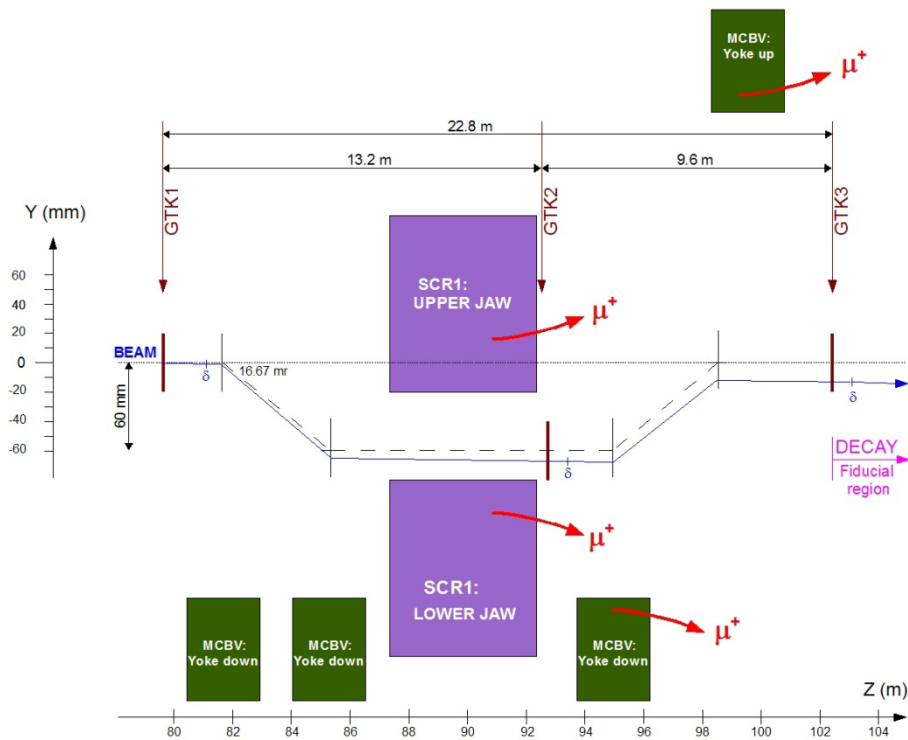


Figure 7 Schematic layout of the beam tracking and momentum-measurement stage (second achromat).

Spatial resolution of one GTK station, $\sigma(x, y) = 0.3 \text{ mm}/12^{1/2} \approx 0.087 \text{ mm}$

Multiple scattering in one GTK station, $\delta(x', y') = 15 \text{ mrad} \cdot (X/X_0 = 4.5 \cdot 10^{-3})^{1/2} / p \text{ (GeV/c)} \approx 0.013 \text{ mrad}$

Measurement Resolutions:

Angle : $\Delta x', \Delta y' \text{ (r.m.s.) (mrad)} = [2 (\sigma/22.8)^2 + \delta^2 + (13.2 \delta/22.8)^2]^{1/2}$

Resolution: GTK1+3, Mult. scatt.: GTK3 GTK2

= ~0.016 mrad

Momentum: $\text{—(r.m.s.) (%) = } [\sigma^2 + (9.6 \sigma/22.8)^2 + (13.2 \sigma/22.8)^2 + (9.6 \times 13.2 \delta/22.8)^2]^{1/2} \times 100/60$

Resolution: GTK2 GTK1 GTK3, Mult. scatt.: GTK2

= ~0.22 %

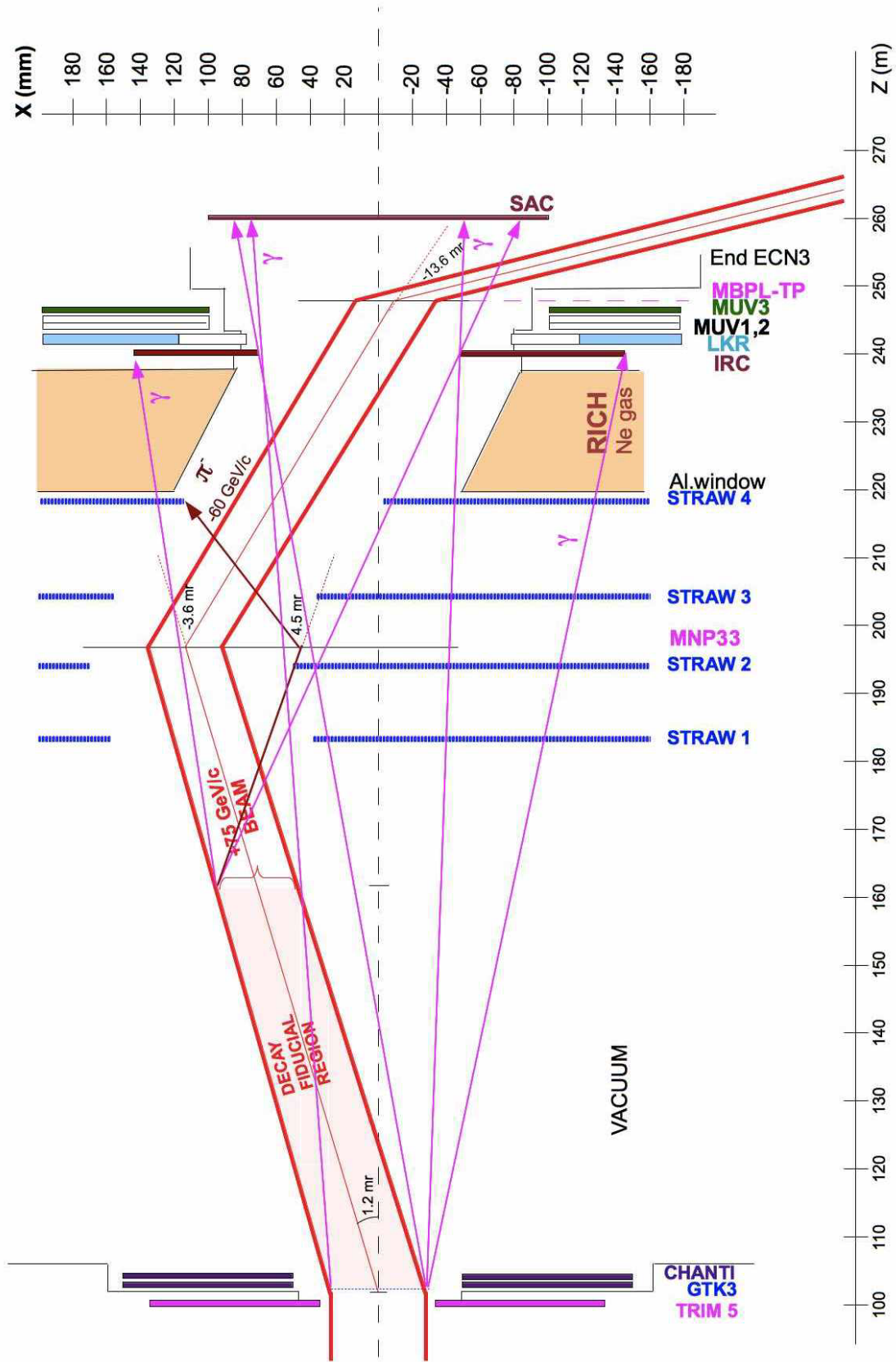


Figure 8 Schematic layout of the downstream part of the beam. Shown is the angular deviation of the charged kaon beam and the 2σ width of the beam profile.

1.1.2.8 Decay Region, Magnetic Spectrometer and Detectors

The decay fiducial region is contained in the first 60m of a large, ~117m long, evacuated tank (described in Chapter 3.1.1), which is closed off by a thin ($\sim 0.045 X_0$) aluminium window, separating it from the neon gas of the following RICH counter. This window is off-set horizontally and its centre is traversed by a thin-walled aluminium beam tube (of inside diameter 155.8mm), which follows the trajectory of the beam, which is thus transported in vacuum through the downstream detectors (Figure 8).

The detector components are described in later Chapters. Of relevance for the beam is the single magnetic spectrometer, comprising four tracking chambers composed of straw-tubes (STRAW 1 - 4), covering the full acceptance outside a ~118mm-wide, empty passage around the beam path. These are interspaced by the existing, large-aperture dipole magnet (MNP33), which provides a horizontal p_T -kick of -270 MeV/c, thereby deflecting the 75 GeV/c beam by -3.6 mrad, so as to converge to the undeviated axis at a point just after the LKR calorimeter. As well as tracking candidate π^+ from K^+ decays, the layout of the spectrometer is designed to detect π^- (from K^+e4 decays) of momenta extending up to 60 GeV/c, deflected through angles $> +4.5$ mrad by MNP33; (a limiting ray is shown in Figure 8).

Near the point of convergence of the beam with the axis following the LKR calorimeter, a pair of 'Big' filament scintillator counters, FISC 5 and 6 (XFBH101245, XFBV101246), allow the beam to be observed and steered correctly. The beam is then deflected to the side through a further angle of -13.6mrad by a 2m-long, 200mm-gap, tapered-pole magnet (MBPL-TP) to reach a point ~12m further downstream, where it clears a small-angle, photon-veto calorimeter (SAC). This is inserted by ~6m on rails into the beam vacuum tube, of 600mm inner diameter. This tube is itself installed in a larger pipe, which is buried in the ground beyond the end of the cavern, ECN3. The beam is finally absorbed in a beam dump composed of iron surrounded by concrete at the downstream end of this pipe, at a distance behind the detector, which allows space to shield against 'back-splash'.

As shown in Figure 8, the detection of photons from the fiducial region is rendered hermetic in the forward direction by an intermediate ring calorimeter (IRC) in front of the LKR calorimeter and a final small-angle calorimeter (SAC). At the IRC, the beam still has a displacement towards positive x with respect to the undeviated axis. The inner aperture of the IRC, chosen to be 120mm in diameter, can thus be centered on the beam with an off-set in x of +12mm. With appropriate alignment (at an angle of -2.0mrad) and a modest increase (to 170mm) in the inner diameter of the upstream end of the vacuum tube traversing the RICH, it thereby becomes possible to assure that photons pointing from the fiducial region towards the SAC will not encounter any material in their path. This feature is vital, since any e^+e^- resulting from conversion would escape detection in the SAC, due to the action of the preceding beam-deflecting magnet.

1.1.2.9 Beam Parameters and estimated Performance

The principal characteristics of the high-intensity K⁺ beam are listed in Table 6, where the parameters determining the flux yield are compared with those for the previous K12 simultaneous K⁺ and K⁻ beam, designed for experiment NA48/2 (3). The effective solid angle and momentum acceptance, as well as the beam sizes and divergences are calculated using the ray-tracing programme TURTLE (10), corresponding to the updated output file accessible from (6). For example, the simulated momentum distribution and the spot sizes at the positions of the three beam tracking detectors (GTK1, 2 and 3) are shown in Figure 9 and Figure 10, respectively. The particle fluxes of the previous beam are taken from the measurements actually made at 60 GeV/c. The relative particle-composition of the 75 GeV/c beam is derived from a scan made with a CEDAR counter in a secondary beam (H2) at the SPS in 2007, whereas the total hadron flux is taken as the average of the values obtained by interpolation from 60 and from 120 GeV/c according to the empirical formula proposed in (1).

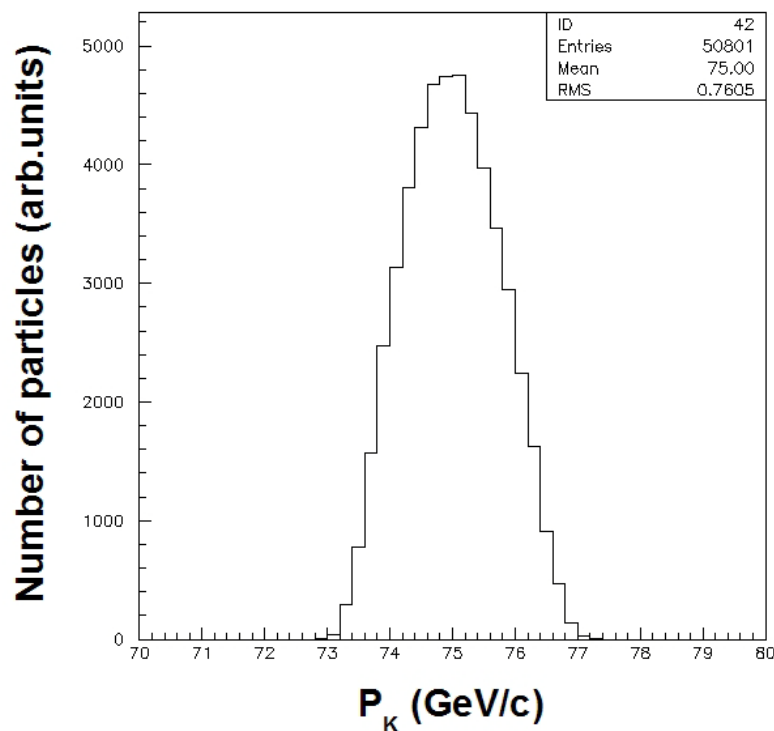


Figure 9 Beam momentum spectrum.

Table 6 High Intensity K^+ Beam for experiment NA62 with 1 X₀ W radiator to suppress e^+ in comparison with previous NA48/2 beam.

Beam Experiment	K12K+K- NA48/2	K12HIKA+ NA62	Comparison FACTOR ¹²
SPS Protons per s of spill length Instantaneous Proton Rate per effective s	$\sim 2 \times 10^{11}$ 3.3×10^{11}	0.7×10^{12} 1.1×10^{12} (equiv. 1.0×10^{12}) ¹³	3.0
SPS Duty Cycle (s / s) Effective Duty Cycle (s / s)	4.8/16.8 = 0.29 ~ 0.18	~ 0.3 ~ 0.2	~ 1.1
Beam Acceptance x_0, y_0 (mrad)	$\pm 0.36, \pm 0.36$	$\pm 2.7, \pm 1.5$	
Solid Angle (μ sterad)	≈ 0.4	≈ 12.7	32
Mean K^+ Momentum $\langle p_K \rangle$ (GeV/c)	60	75	K^+ 1.4 π^+ 1.5 Total Hadrons 1.6
Momentum Band: - Effective $\Delta p/p$ (%) - r.m.s. $\Delta p/p$ (%)	± 5 ≈ 3.7	± 1.65 1.0	0.33
R.m.s. Divergence: x', y' (mrad) at CEDAR		0.07	
2 r.m.s. Beam Size (mm) Area at GTK 3 (mm ²) R.m.s. Divergence: x', y' (mrad)	$r = \sim 15$ ~ 700 $\approx 0.05, 0.05$	$x = \pm 27.5, y = \pm 11.4$ ~ 980 0.09, 0.10	~ 1.4
Decay Fiducial Length: (m) Δz (τ_{K^+}) Decay Fraction: $(1 - e^{-\Delta z})$	50 0.111 0.105	60 0.107 0.101	0.96
Inst. Beam Rate / s (MHz): p K^+ π^+ e^+, μ^+ Total	2.9 1.0 11.1 $\sim 3, \sim 0.13$ ~ 18	173 45 525 $\sim 0.3, \sim 6$ 750	60 45 47 $\sim 0.1, \sim 45$ ~ 42
Fraction of hadrons in GTK 1 GTK 1 + 2 + 3 Mean Rate over sensitive area of KABES / GTK3 (kHz / mm ²) Maximum Rate per Si pixel (kHz / [0.3 x 0.3] mm ²)	~ 25	0.987 0.981 463 114	~ 19
Overall Efficiency x Running Time/year (days /yr.) Effective Spill Time/year (s /yr.)	0.5 $\times 120 = 60$ 9.3×10^5	0.6 $\times 100 = 60$ 1.0×10^6	~ 1.1
K^+ Decays per year in fiducial length	1.0×10^{11}	4.5×10^{12}	≈ 45

¹² The comparisons refer to the positive beam only of the simultaneous $K^+ + K^-$ beams for experiment NA48/2.

¹³ The equivalent instantaneous proton beam rate of $(1.0 \times 10^{12}) \text{ s}^{-1}$ takes into account the 10% loss of secondary hadrons from the K12HIKA+ beam due to absorption and multiple scattering in the 1 X₀ W radiator, introduced to suppress the e^+ component. This equivalent proton rate is used for the comparison FACTOR.

The muons accompanying a high-energy, high-intensity, secondary beam contribute a major part of the single-particle flux, to which the detectors outside the beam are exposed. The transport and decay to $\mu^\pm \nu$ of a wide spectrum of π^\pm and K^\pm originating in the target has been simulated using the programme *HALO* (11), corresponding to the four updated output files accessible from (6). The programme tracks the parent particles and their decay muons inside the beam apertures and the 'halo' muons leaving the apertures through the vacuum tubes, magnet yokes and shielding surrounding the beam. Results of such calculations are given in Table 7 and Table 8. As an example, the distribution of halo muons traversing a plane of vertical straw tubes in STRAW chamber 4 is plotted in Figure 11.

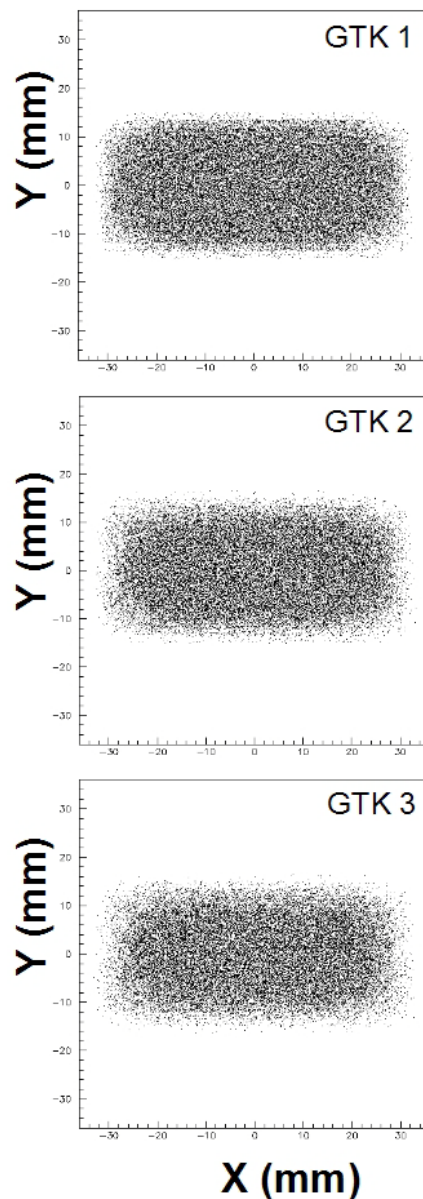


Figure 10 Spot-sizes of the high intensity K+ beam in the three Gigatracker stations.

Table 7 Estimated Muon Halo in the K12HIKA+ Beam

INSTANTANEOUS RATES x 10⁶ from 1.1 10¹² incident protons per eff. s¹⁴	π^+ → $\mu^+ \nu$	K^+	π^- → $\mu^- \bar{\nu}$	K^-	TOTAL
π, K at GTK 3 (z = 102.4m)	525	45	0	0	570
μ in beam at GTK 3	4.38	0.46	0	0	4.84
μ 'HALO' at GTK 3 reaching LKR cal.	1.66	0.65	0.15	0.01	2.47
μ at CEDAR PMT's: 25<r<30cm (z=69.3m)	4.16	0.35	0.76	0.10	5.37
μ in GTK Guard Ring CHANTI: 4.5< x <15, 2.5< y <15cm ANTI-HALO counter: r > 18, x , y < 60 cm (z=104.1m)	1.26	0.62	0.04	0.01	1.93
	1.47	0.33	0.64	0.10	2.54
Large Angle Veto: LAV 1 (z=121.4m)	1.13	0.25	0.28	0.05	1.71
LAV 1-12 - TOTAL	5.88	3.52	1.26	0.25	10.91
LAV 1-12 - OR	1.93	1.52	0.46	0.12	4.03
μ per plane of STRAW 1 (z=183.5m) [210 x 210] cm ² , x > 5.9 cm	2.11	4.00	0.21	0.02	6.34
[210 x 210] cm ² , y > 5.9 cm	2.53	4.13	0.25	0.02	6.93
STRAW 2 (z=194.1m)	2.22	4.40	0.21	0.01	6.84
[210 x 210] cm ²	2.58	4.59	0.22	0.01	7.40
STRAW 3 (z=204.5m)	2.18	4.72	0.20	0	7.10
[210 x 210] cm ²	2.57	4.92	0.21	0.01	7.71
STRAW 4 (z=219.1m)	2.89	4.82	0.15	0.01	7.87
[210 x 210] cm ²	2.77	5.08	0.16	0.01	8.02
RICH: 12 < r < 120 cm (z=237.35m)	2.27	5.67	0.15	0.01	8.10
IRC: 6 (x=+1.2cm) < r < 14.5 cm (z=239.7m)	6.62	1.02	0	0	7.64
CHOD/ LKR: 12<r< 120 cm (z=241.08m)	2.78	5.80	0.15	0.01	8.74
MUV: r > 12, x , y < 140 cm (z=246.5m)	4.39	6.30	0.18	0.02	10.89
SAC: [20 x 20] cm ² (z=261.0m)	0.04	0.13	0	0	0.17

¹⁴ The statistics of the simulation are such that each ray tracked represents 10⁴ particles.

Table 8 Expected instantaneous muon rates in the detectors - for 1.1×10^{12} protons per effective second of spill

DETECTOR	Area (cm ²)	K12 HIKA+ BEAM TOTAL RATE (MHz)	MAXIMUM INTENSITY / effective s (kHz/cm ²)	Annual MUON dose rate (Gy per year) ¹⁵
CEDAR PMT's: (25<r<30cm)	864	5.4	~10	~5
GTK 3 Guard Ring:				
- CHANTI: 4.5< x <15cm 2.5< y <15 cm	855	1.9	~4	~2
- ANTI-HALO counter: r>18, x , y <60cm	1.34 x 10 ⁴	2.5	~0.2	~0.1
Large Angle Veto:				
- LAV 1	1.67 x 10 ⁴	1.7	~0.1	~0.05
- LAV 1-12 TOTAL	26.0 x 10 ⁴	10.9		
- LAV 1-12 OR	26.0 x 10 ⁴	4.0		
STRAW Chamber 4:				
- per plane: 5.9 < x < 105 cm 5.9 < y < 105 cm	4.16 x 10 ⁴ 4.16 x 10 ⁴	7.9 8.0		
- per Ø 1 cm STRAW: (5.9< x <6.9)x210cm (5.9< y <6.9)x210cm	210 210	0.5 0.4	~30	~15
RICH: (12 <r< 120cm)	4.48x10 ⁴	8.1		
IRC: 6 (x=+1.2cm)<r< 14.5cm	547	7.6	~80	~40
CHOD / LKR cal.:				
- 12 <r< 120cm	4.48x10 ⁴	8.7		
- 12 <r< 16cm	352	1.3	~4	~2
MUV: r>12, x , y <140cm	7.79 x 10 ⁴	10.9		
SAC: (20x20) cm ²	400	0.17	~0.4	~0.2

¹⁵ 1 Gy = 1 J/kg = 6.24×10^9 MeV/g = $[6.24 \times 10^9 / (dE/dx)]$ charged particles / cm².

Taking $dE/dx \sim 1.8$ MeV/g cm² for minimum-ionizing charged particles traversing the detectors, 1 Gy/year = $\sim 3.5 \times 10^9$ $\mu\pm$ / cm² / year.

This translates to a maximum intensity of $\sim 2 \times 10^3$ $\mu\pm$ / cm² / effective second of spill integrated over a year of $\sim 1.7 \times 10^6$ eff.s (100 days x 0.2 eff. duty cycle)

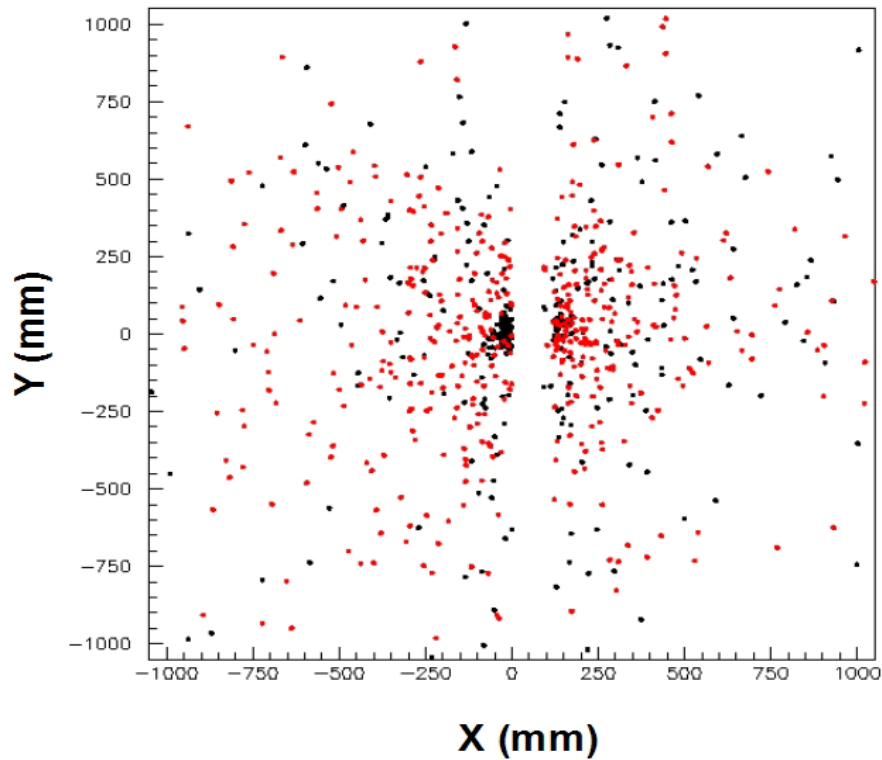


Figure 11 Simulated distribution of the muon halo - traversing a plane of vertical straw tubes ($6 < |x| < 105\text{cm}$) in STRAW chamber 4. One entry in the histogram represents $10^4 \mu^\pm$ from $\pi^+, (\pi^-) \rightarrow \mu^{+(-)}$ decays (black dots), K^+ and $(K^-) \rightarrow \mu^{+(-)} \nu$ decays (red dots) - per $1.1 \cdot 10^{12}$ incident protons per effective second of spill.

1.1.2.10 SPS Scheduling and Proton Availability

From the parameters in Table 6 we conclude that, with effective overall data-taking efficiency (SPS and experiment) of 0.6, $K^+ \rightarrow \pi^+ \nu \bar{\nu}$ branching ratio of 1×10^{-10} and detector acceptance of 0.1, **~45 events** could be accumulated in **~2.5 x 10⁶ seconds** of 400 GeV/c slow-extracted proton beam on target (equivalent to $\sim 1.7 \times 10^6$ effective seconds of spill). With a duty cycle of 0.3 (~ 0.2 effective), this could be provided in a year of ~ 100 days of scheduled fixed-target proton physics.

The instantaneous primary beam rate assumed is 1.1×10^{12} protons on target T10 per effective second of spill, corresponding to a mean rate of $\sim 0.7 \times 10^{12}$ per real second of flat-top for slow-extraction at 400 GeV/c momentum.

Thus, for example, with an SPS cycle giving 9.6 real seconds of flat-top per pulse, this would correspond to $\sim 7 \times 10^{12}$ protons per pulse (ppp) onto target T10. With a 300mm-long beryllium target generally used in the upstream target station T4, this would require $\sim 1.8 \times 10^{13}$ ppp to be directed into the branch from the 3-way split towards T4.

The proton flux needed at T4 might be reduced to $\sim 1.0 \times 10^{13}$ ppp, if the proton beam, instead of being focused onto the target in both planes, were to be rendered parallel in the vertical plane with an extent of ~ 10 mm. Then the 2mm-high T4 target would intercept only $\sim 20\%$ of the protons, allowing the remaining $\sim 80\%$ to by-pass the target without absorption. A study has shown that the front-end optics of the P42 beam line to T10 could be adapted according to this scheme.

1.1.2.11 Future Beam Options

The layout and optics of the K12HIKA+ beam are optimised to provide the high-intensity, single-charge beam required by the $K^+ \rightarrow \pi^+ \nu \bar{\nu}$ experiment NA62.

However, in adopting a ‘straight-line’ layout from the existing target station T10 to the LKR calorimeter, two further options have been built in to the front-end of the beam. These have been included in the combinations of K12 beam dump/collimator (TAX 1 and 2) positions listed in Table 4 and are illustrated in Figure 4 (c) and (d), respectively :

- 1) Simultaneous, positively- (K^+) and negatively-charged (K^-) beams of hadrons with momenta up to $\sim \pm 75$ GeV/c could be selected, following ‘DOWN’ and ‘UP’ paths through the front-end achromat (Figure 4 (c)). The first triplet of quadrupoles (with D-F-D polarities)¹⁶ could be tuned to bring the two beams to foci, having similar, first-order, magnifications in both planes, at the point of momentum-selection in the middle of the front-end achromat. The second quadrupole triplet (with D-F-D polarities) could then bring the beams to a common, second focal point, where differences in the cumulative, second-order (notably ‘chromatic’) aberrations would almost cancel. A subsequent (new) sequence of four quadrupoles (with D-F-D-F polarities), placed upstream of the second achromat, could be arranged to give the two beams similar lateral sizes and (small) divergences entering the fiducial region leading to the detectors. Moreover, the e^\pm radiator mechanism in the front-end achromat Figure 5 is designed to intercept both beams and to suppress the e^+ and e^- components by similar factors.
- 2) A high-intensity, neutral beam (K12HIK0L), with angular acceptance up to $\sim \pm 0.2$ mrad in each plane, could be selected along the straight, undeviated axis (in Figure 4 (d)). The beam could be simply derived from the primary proton beam at zero production angle, or, if the first three quadrupoles and one steering dipole magnet are removed, it could be produced at a (vertical) angle of ~ 2.5 mrad, to yield a more optimum ratio of the K_L^0 / neutron content.

¹⁶The focusing sequence of the quadrupoles refers to their action on the positive beam in the horizontal plane and is similarly valid for the negative beam in the vertical plane. Therefore, to obtain two beams of opposite charge having similar characteristics, the focusing action of the quadrupoles on each beam must be made similar in the horizontal and vertical planes. In addition, there is a weak effect due to the fringe fields at the ends of the rectangular poles of the vertically-deflecting dipole magnets in the front-end and in the second achromats. This effect results in a small extra focusing in the horizontal plane, which is similar for the two beams.

In both cases, however, the layout of straws, in each of the four STRAW chambers and the alignment of the RICH counter (Figure 8), would have to be modified to exploit such beams. Otherwise the beams would intercept these detectors.

Bibliography

1. **Atherton H. W. , et al.** *Precise Measurements of Particle Production by 400 GeV/c Protons on Beryllium Targets.* Geneva : s.n., 1980. CERN Yellow Report: CERN 80-07.
2. **NA48 Collaboration; Anvar, S. et al.** The Beam and Detector for the NA48 neutral kaon CP violation experiment at CERN. *Nucl. Instrum. Methods A 574.* 2007, pp. 433-471.
3. **The NA48/2 collaboration; Batley J. R. et al.** Search for direct CP violating charge asymmetries in $K_{\pm} \rightarrow \pi^{\pm} \pi^+ \pi^-$ and $K_{\pm} \rightarrow \pi^{\pm} \pi^0 \pi^0$ decays. *Eur. Phys. J. C 52.* 2007, pp. 875-891.
4. **Brianti, G. et Doble, N.** *The SPS North Area High Intensity Facility: NAHIF.* CERN. Geneva : s.n., 1977. SPS/EA 77-2; SPSC/T-18.
5. **Bonnet, Y.** *Layout TCC2/TT81--->85.* CERN. Geneva : s.n., 2006. CERN Drawing Directory (CDD) : SPSXLTC20001.
6. **Doble, N.** Beam Documentation for NA48/NA62: Geometry-BEATCH, Optics-TRANSPORT, Beam Simulations-TURTLE and HALO. *CERN.* [En ligne] 2010. <http://doble.web.cern.ch/doble/>.
7. **Y., Bonnet.** *Layout TCC8/ECN3.* CERN. Geneva : s.n., 2009. CERN Drawing Directory (CDD); SPSXLECN0002.
8. **Brown K.L., et al.** *TRANSPORT, A Computer Program for designing Charged Particle Beam Transport Systems.* Geneva : s.n., 1980. CERN Yellow Report: CERN 80-04.
9. **Bovet C. et al.** *The CEDAR counters for Particle Identification in the SPS Secondary Beams.* CERN. Geneva : s.n., 1982. CERN Yellow Report : CERN 82-13.
10. **Brown, K.L. et Iselin, Ch.** *DECAY TURTLE, A computer Program for simulating Charged Particle Beam Transport Systems.* Geneva : s.n., 1974. CERN Yellow Report: CERN 74-2.
11. **Iselin, Ch.** *HALO, A Computer Program to calculate Muon Halo.* Geneva : s.n., 1974. CERN Yellow Report: CERN 74-17.
12. **P.S. Cooper et al.** *Charged Kaons at the Main Injector.* FNAL. Chicago : s.n., 2001.